Title

Photoenhanced metastable c-axis electrodynamics in stripe-ordered cuprate $La_{1.885}Ba_{0.115}CuO_4$.

Journal

Proceedings of the National Academy of Sciences of the United States of America, 116(40)

ISSN

0027-8424

Authors

Cremin, Kevin A
Zhang, Jingdi
Homes, Christopher C
et al.

Publication Date

2019-10-01

DOI

10.1073/pnas.1908368116

Peer reviewed

Photoenhanced metastable c-axis electrodynamics in stripe-ordered cuprate $La_{1.885}Ba_{0.115}CuO_4$

Kevin A. Cremin[a,1], Jingdi Zhang[a,b,1], Christopher C. Homes[c], G. D. Gu[c], Zhiyuan Sun[a,d], Michael M. Fogler[a], Andrew J. Millis[d,e], D. N. Basov[d], and Richard D. Averitt[a,2]

[a]Department of Physics, University of California San Diego, La Jolla, CA 92093; [b]Department of Physics, Hong Kong University of Science and Technology, Clear Water Bay, Kowloon, Hong Kong, China; [c]Condensed Matter Physics and Materials Science Department, Brookhaven National Laboratory, Upton, NY 11973; [d]Department of Physics, Columbia University, New York, NY 10027; and [e]Center for Computational Quantum Physics, Flatiron Institute, New York, NY 10010

Edited by Angel Rubio, Max Planck Institute for the Structure and Dynamics of Matter, Hamburg, Germany, and approved August 20, 2019 (received for review May 15, 2019)

Quantum materials are amenable to nonequilibrium manipulation with light, enabling modification and control of macroscopic properties. Light-based augmentation of superconductivity is particularly intriguing. Copper-oxide superconductors exhibit complex interplay between spin order, charge order, and superconductivity, offering the prospect of enhanced coherence by altering the balance between competing orders. We utilize terahertz time-domain spectroscopy to monitor the c-axis Josephson plasma resonance (JPR) in $La_{2-x}Ba_xCuO_4$ ($x = 0.115$) as a direct probe of superconductivity dynamics following excitation with near-infrared pulses. Starting from the superconducting state, c-axis polarized excitation with a fluence of 100 μJ/cm^2 results in an increase of the far-infrared spectral weight by more than an order of magnitude as evidenced by a blueshift of the JPR, interpreted as resulting from nonthermal collapse of the charge order. The photoinduced signal persists well beyond our measurement window of 300 ps and exhibits signatures of spatial inhomogeneity. The electrodynamic response of this metastable state is consistent with enhanced superconducting fluctuations. Our results reveal that $La_{2-x}Ba_xCuO_4$ is highly sensitive to nonequilibrium excitation over a wide fluence range, providing an unambiguous example of photoinduced modification of order-parameter competition.

superconductivity | cuprates | charge ordering

High-temperature superconductivity in the cuprates can coexist or compete with a multitude of other phenomena, including charge and spin order, pair density waves, and the pseudogap (1–4), all of which have observable signatures in the linear or transient electrodynamic response (5). A key question for the cuprates is the extent to which the underlying interactions can be manipulated to alter the macroscopic properties. Ultrafast pump–probe spectroscopy provides a unique means to initiate and interrogate nonequilibrium dynamics and property control in superconductors (6, 7).

Evidence of transiently enhanced interlayer tunneling has been reported in several cuprates following selective phonon pumping (8–10) or intense near-infrared excitation (11). In these experiments, the c-axis Josephson plasma resonance (JPR) serves as a reporter of the interlayer tunneling which, in general, scales with the superfluid spectral weight (12). Upon applying intense near-infrared pump excitation starting above the transition temperature T_c, Nicoletti et al. (11) observed a blueshift of the plasma resonance relative to the below T_c equilibrium response. The plasma resonance decayed after several picoseconds and was interpreted in terms of transient superconductivity. Similar dynamics were subsequently observed in both $La_{2-x}Ba_xCuO_4$ and $YBa_2Cu_3O_{6+x}$ over a range of doping levels and excitation conditions. More recently, in $La_{2-x}Ba_xCuO_4$ ($x = 0.095$), a longer-lived (>50 ps) collective response was observed subsequent to photoexcitation at $T < T_c$ in which the JPR appeared to split into 2 distinct longitudinal modes (13), reminiscent of the static electrodynamic response in bilayer cuprates (14–16). Further, no pump-induced effect was observed above T_c. Notably, the $x = 0.095$ material does not exhibit robust charge or stripe order (17).

In this report, we clarify the details of the photoinduced order parameter control in the cuprates, by performing temperature and fluence-dependent c-axis measurements on materials with equilibrium signatures of phase competition. We present near-infrared pump, THz probe experiments of $La_{2-x}Ba_xCuO_4$ ($x = 0.115$), for which we observe distinct dynamics above and below T_c. The doping $x = 0.115$ is close to the anomalous $x = 1/8$ composition where 3D superconductivity is maximally suppressed by robust charge and stripe order (2, 18–20). At $x = 0.115$, charge order, spin order, and 3D superconductivity onset at $T_{co} = 53$ K, $T_{so} = 40$ K, and $T_c = 13$ K, respectively (17). In this compound T_c is high enough to enable initiating dynamics from within the superconducting state. The $La_{1.885}Ba_{0.115}CuO_4$ crystal was cut and polished to expose the *a-c* plane with a large area of 5 mm × 5 mm. Temperature-dependent Fourier transform infrared spectroscopy (FTIR) measurements were carefully performed to provide a baseline static characterization of the electrodynamic response (see *SI Appendix*, section S1 for details).

The static and dynamic reflectivity of LBCO were measured as a function of temperature and fluence using terahertz time-domain

Significance

The emergence of superconductivity in high-temperature cuprates arises out of a rich landscape of competing order. For example, stripe order can hoard the electrons needed to form Cooper pairs and establish superconductivity. Intriguingly, the complex interactions of such intertwined orders can be manipulated with light, where nonequilibrium dynamics alter the primacy of one order over another. Following photoexcitation of $La_{2-x}Ba_xCuO_4$ ($x = 0.115$) with near-infrared pulses, we observe a long-lived state that exhibits enhanced superconducting correlations well above the equilibrium superconducting transition temperature. Our analysis reveals that this metastable phase arises from a collapse of stripe order, providing an important demonstration of light-directed control in quantum materials.

Author contributions: K.A.C., J.Z., D.N.B., and R.D.A. designed research; K.A.C., J.Z., C.C.H., G.D.G., Z.S., M.M.F., and A.J.M. performed research; K.A.C. and Z.S. analyzed data; D.N.B. and R.D.A. provided overall guidance on the project; K.A.C. and R.D.A. wrote the paper with input from all authors.

The authors declare no conflict of interest.

This article is a PNAS Direct Submission.

Data deposition: The data that support the findings of this study are available from the authors on request.

[1]K.A.C. and J.Z. contributed equally to this work.

[2]To whom correspondence may be addressed. Email: raveritt@ucsd.edu.

This article contains supporting information online at www.pnas.org/lookup/suppl/doi:10.1073/pnas.1908368116/-/DCSupplemental.

First published September 16, 2019.

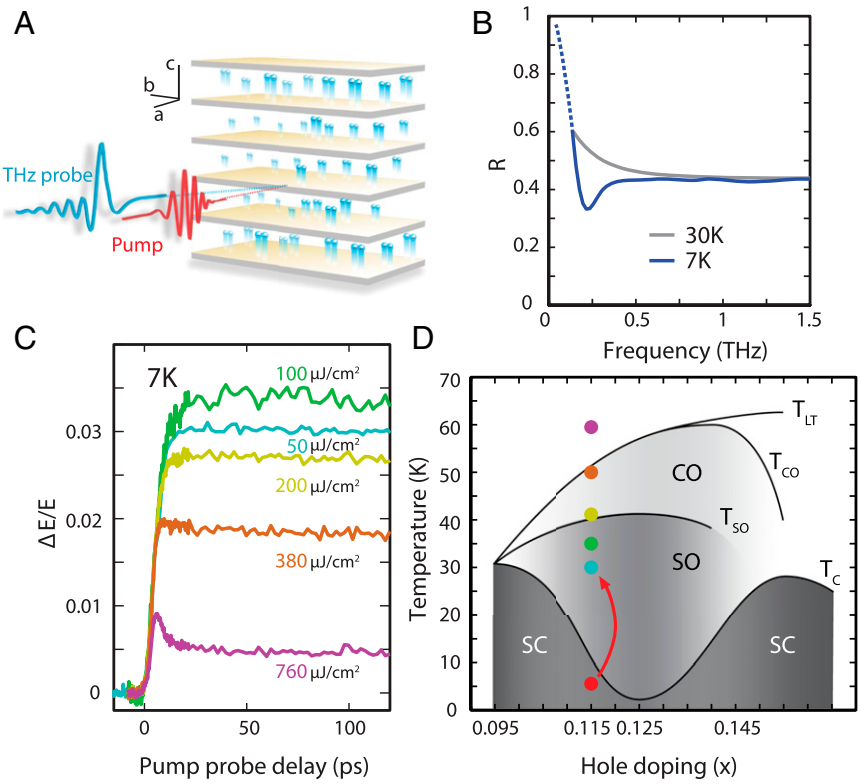

Fig. 1. (*A*) Schematic of the 1.55-eV pump THz probe experiment on LBCO crystal with pump and probe polarization along c axis. The illustration depicts the superconducting state with electron pairs tunneling along the c axis. (*B*) Equilibrium THz reflectivity above and below T_C at 30 and 7 K, respectively. The dotted line is beyond our experimentally accessible spectral range and is a guide to the eye. (*C*) Time-dependent relative change in the THz electric field amplitude after excitation at various pump fluences (at 7 K). (*D*) Temperature versus hole doping phase diagram of $L_{2-x}Ba_xCuO_4$. Adapted with permission from ref. 17. Regions of the phase diagram include bulk superconductivity (SC) at onset temperature T_c, spin ordering (SO) at temperature T_{so}, charge ordering at T_{co}, and low-temperature structural transition T_{LT}. The initial temperature at 7 K for x = 0.115 is plotted in red, and the color dots mark the estimated lattice temperature after pump excitation and e-ph thermalization has occurred (colors corresponding to pump fluences shown in *C*).

spectroscopy (0.15 to 2 THz). As shown in Fig. 1*A*, both the near-infrared pump (1.55 eV) and the THz probe pulses are polarized along the c axis. The static THz reflectivity is plotted in Fig. 1*B*, showing a flat response at 30 K (gray line, with a slight upturn below 0.5 THz). In the superconducting state (7 K, blue curve) a sharp reflectivity edge emerges around 200 GHz, a hallmark of the interlayer JPR effect in agreement with previous studies for this doping (11).

For the dynamics measurements, we first performed 1-dimensional scans, where the photoinduced change in the peak electric field of the single-cycle THz pulse (ΔE/E) is measured as a function of pump-probe delay. These raw unprocessed data unambiguously highlight important features of the electrodynamic response. Fig. 1*C* plots 1-dimensional scans (ΔE/E peak scans) for various fluences, starting from an initial temperature of 7 K, well into the superconducting state. The dynamics exhibit a long-lived response with an initial risetime of several picoseconds. The magnitude of the ΔE/E signal slightly increases from 50 to 100 μJ/cm^2, followed by a strong decrease in amplitude at higher fluences up to 760 μJ/cm^2. The observed fluence dependence indicates dynamics that are distinct from a photoinduced decrease in the condensate density with a commensurate increase in the quasiparticle density. In that scenario, ΔE/E would increase in magnitude with increasing fluence.

Calculations using the 2-temperature model of the initial electron-phonon (e-ph) thermalization (see *SI Appendix*, section S3 for details) indicate a rise in the final temperature that increases with fluence (after several picoseconds when the plateau in the data in Fig. 1*C* is reached). Fig. 1*D* displays the phase diagram of LBCO (reproduced from ref. 17) with color-coded dots (corresponding to the fluences used in Fig. 1*C*) indicating the final temperature after thermalization. Clearly, the amplitude of ΔE/E decreases with increasing fluence as T_{co} is approached after the initial e-ph thermalization. This indicates that the strongest photoinduced response occurs for fluences that do not heat the sample above T_{co}. We refer to 50 to 380 μJ/cm^2 as the low-fluence regime where the quasiequilibrium temperature stays below T_{co}. The data in Figs. 2 and 3 reveal that the dynamics are dramatically different for low- and high-fluence (>380 μJ/cm^2) regimes spanning T_{co}. The difference in dynamics is evident in Fig. 1*C*, where the 760-μJ/cm^2 data exhibit an exponential decay in contrast to the plateau apparent in the low-fluence data.

We now discuss the full spectroscopic response of the dynamics, considering first low-fluence optical excitation of LBCO (100 μJ/cm^2) obtained starting from an initial temperature of 7 K. The optical properties of the photoexcited region were extracted using a layered model to account for the penetration depth mismatch between the pump and probe beams (see *SI Appendix*, section S2). Fig. 2*A* shows the photoinduced reflectivity (blue curve at 10 ps, red curve at 300 ps), revealing a large reflectivity increase extending out to 1 THz, corresponding to an increase in the plasma frequency from ∼0.2 to 0.9 THz. This is more clearly revealed in Fig. 2 *B* and *C* showing the loss function $-\mathrm{Im}(1/\varepsilon)$ (where $\varepsilon = \varepsilon_1 + i\varepsilon_2$ is the c-axis dielectric response) which peaks at the plasma frequency. Importantly, there is no sign of decay of the photoinduced state over the measured temporal window, indicating a metastable state that persists beyond 300 ps. Fig. 2 *D* and *E* show the associated c-axis optical conductivity ($\sigma = \sigma_1 + i\sigma_2$) highlighting an important observation. Namely, there is a peak in σ_1 at 0.3 THz signifying

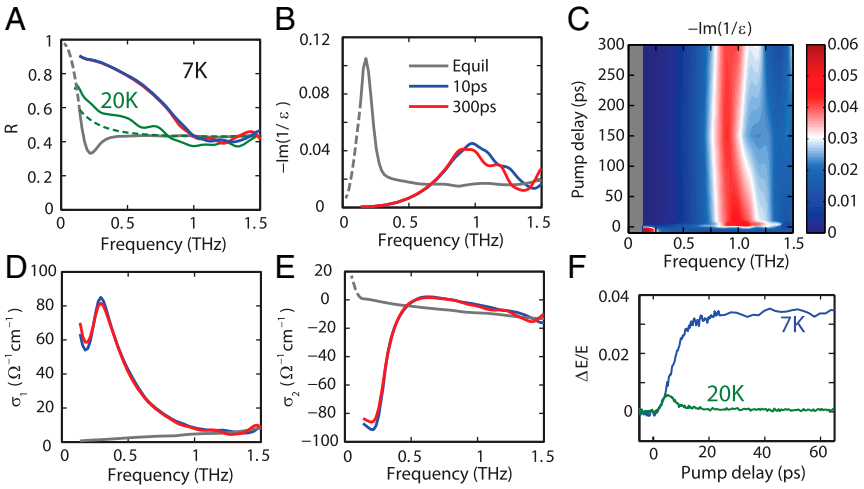

Fig. 2. Extracted c-axis THz optical properties of LBCO at different pump–probe delays after photoexcitation (colored) with 100 μJ/cm^2 and at equilibrium (gray). All data have been taken at 7 K below T_C except for the green curves in *A* and *F* which were taken at 20 K. (*A*) Reflectivity at 7 K before (gray) and after photoexcitation (colored) at different pump–probe delays. Plotted in green is the equilibrium (dotted) reflectivity and largest photoinduced change (solid) in reflectivity at 20 K. (*B*) Loss function −Im(1/ε). Dashed gray line is beyond our spectral resolution and is a guide to the eye. (*C*) Spectral evolution of the loss function after photoexcitation. (*D* and *E*) Real and imaginary parts of the THz conductivity. (*F*) Peak of ΔE/E THz transient after photoexcitation at 7 and 20 K.

dissipation in the c-axis THz transport. In contrast, in equilibrium for a superconductor, σ_1 at frequencies greater than zero but less than twice the superconducting gap approaches zero (solid gray line in Fig. 2*D*). This origin of the peak in σ_1 arising after photoexcitation will be discussed below. Finally, the solid green line in Fig. 2*A* shows the spectral response at 10 ps delay for a fluence of 100 μJ/cm^2 taken at an initial temperature of 20 K—that is, above T_c. There is an increase in the reflectivity, arguably with the development of a weak plasma edge. However, as shown in Fig. 2*F*, the response is much smaller and shorter lived in comparison to dynamics initiated from within the superconducting state. In short, the emergence of a robust metastable state upon low-fluence photoexcitation requires starting from the superconducting state while remaining below T_{co} after e-ph thermalization.

To complete the data discussion, we now consider the high-fluence dynamics. Fig. 3 shows the spectroscopic results for high-fluence excitation at 9 mJ/cm^2 which leads to a final temperature greater than T_{co}. Fig. 3*A* reveals an increased reflectivity starting from an initial temperature of 30 K. At early times a broad peak emerges in the loss function (shown in Fig. 3 *B* and *C*) that rapidly broadens and decays on an ∼10-ps timescale. There is a corresponding increase in σ_1 and σ_2 (Fig. 3 *D* and *E*), although there are no well-defined peaks as for the low-fluence results. Fig. 3*F* reveals the rapid decay in the transient ΔE/E with 9-mJ/cm^2 excitation, with the inset showing a saturation of the dynamics with increasing fluence. The plateau in the ΔE/E scans following the initial exponential decay is presumably associated with heating, leading to a broad and featureless optical conductivity from 0.1 to 1.5 THz. The broadened plasma edge that appears after the arrival of the pump pulse is qualitatively in agreement with the previous study by Nicoletti et al. (11). Given the relatively small value of σ_1, this could indicate the presence

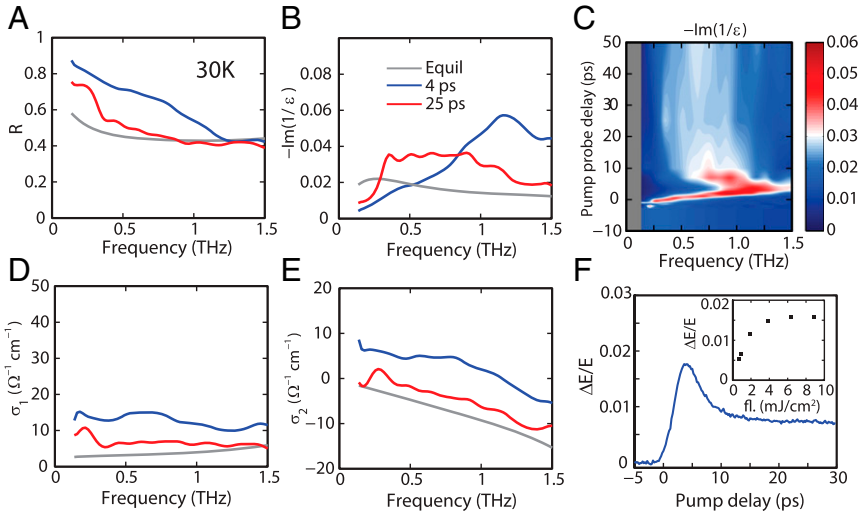

Fig. 3. Extracted c-axis THz optical properties of LBCO at different pump–probe delays after photoexcitation (colored) with 9 mJ/cm^2 and at equilibrium (gray). All data taken at 30 K above T_C and below T_{CO}. (*A*) Reflectivity and (*B*) loss function, −Im(1/ε) at different pump–probe delays. (*C*) Spectral evolution of the loss function after photoexcitation. (*D* and *E*) Real and imaginary parts of the THz conductivity at different pump–probe delays. (*F*) Time-dependent relative changes in THz electric field after photoexcitation. (*Inset*) Display of maximum ΔE/E value at 30 K as a function of pump fluence.

of enhanced superconducting correlations associated with the unambiguous transient blueshift of the plasma frequency. Summarizing, the high-fluence transient response evolves at temperatures above T_{co} and is short-lived in contrast to the low-fluence metastable results presented in Fig. 2, implying that the 2 features correspond to distinct states.

We now discuss the origin and nature of the low-fluence photoinduced metastable electrodynamic response (Fig. 2). For 100 μJ/cm^2, the temperature following e-ph thermalization is ~35 K. In equilibrium, 35 K is within the charge-ordered, nonsuperconducting region that is spectrally featureless at THz frequencies. In contrast, the low-fluence metastable state produced by c-axis excitation exhibits unique spectroscopic features in the loss function $-\mathrm{Im}(1/\varepsilon)$ (Fig. 2 *B* and *C*) and conductivity (Fig. 2 *D* and *E*) that are indicative of a nonequilibrium metastable state. Importantly, the plasma frequency (ω_p) is blueshifted by a factor of 4.5 upon photoexcitation (from 0.2 → 0.9 THz) corresponding to an increase of the low-energy spectral weight (Σ) by a factor of 20 (i.e., $\Sigma \propto {}_p^2$). This is a robust observation, independent of the microscopic origin of the electrodynamic response. Additionally, the spectral weight must originate from energies beyond the 1.5-THz regime probed here because the equilibrium condensate spectral weight (Fig. 4*A*) is far too small to account for the factor of 20 increase. A change in the c-axis response may also arise from structural distortions affecting interlayer coupling independent of a change in the in-plane superfluid density (21). Although our measurements are not directly sensitive to structural distortions, we estimate the metastable phase to be at ~35 K which is still below the low-temperature orthorhombic to tetragonal transition occurring at 53 K (22). As such, this is not likely to be the cause of the increase in Σ. We next show that a more likely scenario for the increase in Σ is photoinduced collapse of charge/stripe order whereby spectral weight originally at energies above the charge density wave (CDW) gap scale is made available for enhanced c-axis transport.

A well-known approximate scaling relationship (valid for both c-axis and ab plane) for the cuprates is $\rho_o = 120\sigma_{dc}T_c$, where ρ_o is the superfluid density ∝(2) and σ_{dc} is the zero-frequency conductivity measured just above T_c (23). Fig. 4*A* shows the product $\sigma_{dc}T_c$ versus ρ_o for x = 0.115 doping measured in this study, and for x = 0.95 and x = 0.145 taken from ref. 22 For x = 0.115 at 7 K, the JPR appears near the renormalized superconducting plasma frequency $\omega'_p = 6.7$ cm^{-1} (200 GHz). The unscreened plasma frequency is given by $\omega_p = \omega'_p\sqrt{\varepsilon_\infty}\varepsilon_\infty \sim 30$ giving a superfluid density $\rho_o \equiv \omega_p^2 = 1.3 \times 10^3$ cm^{-2} (This is taken to be very near the superfluid density at T = 0 K.) The conductivity just above $T_c = 13$ K is taken as $\sigma_{dc} \sim 0.8\ \Omega^{-1}\cdot$cm^{-1}, estimated from transport measurements on a similar doping of x = 0.11 (24). As seen in Fig. 4*A*, the x = 0.115 doping is consistent with $\rho_o = 120\ \sigma_{dc}T_c$ plotted as a dashed line. We now extend this concept to the photoinduced metastable state which, as described above, exhibits a large increase in spectral weight.

From the photoinduced blueshift of the plasma edge ($\omega'_e \sim 0.9$ THz or 30 cm^{-1}) it is possible to determine the photoinduced density ρ_e. This estimate from experimental data gives $\rho_e = 2.7 \times 10^4$ cm^{-2}, yielding $\rho_e/\rho_o \sim 20$ as mentioned above. We now assume the validity of the scaling relation $\rho_e = 120\ \sigma_{co}T_{co}$ where $\sigma_{co} \sim 3\ \Omega^{-1}\cdot$cm^{-1} is the conductivity just above the charge-ordering temperature ($T_{co} = 53$ K). From this we obtain $\rho_e/\rho_o \sim \sigma_{co}T_{co}/\sigma_cT_c \sim 15$, in reasonable agreement with experiment. The product $\sigma_{co}T_{co}$ is plotted in Fig. 4*A* as a red data point and lies on the dashed line given by $\rho_s = 120\ \sigma_{dc}T_c$. This suggests that c-axis spectral weight initially tied up in charge order is released upon photoexcitation leading to the blueshift of the plasma edge. We note that the precise microscopic reason for the photoinduced collapse of charge order upon c-axis interband excitation is not understood and is a topic for future investigation, beyond the scope of the present study.

The peak in the loss function cannot be simply described as an enhanced plasma edge with increased interlayer tunneling arising from the collapse of the charge order. This is because we have a peak in σ_1 at a nonzero frequency (Fig. 2*D*). In principle, 2 inequivalent junctions (with different interlayer spacing) do yield 2 distinct longitudinal JPRs at different frequencies. For example, Sm-doped $La_{2-x}Sr_xCuO_4$ (LSCO), is composed of a stack of inequivalent Josephson junctions. Out-of-phase oscillations of the 2 longitudinal modes result in a transverse mode with a resonance frequency intermediate to the 2 JPRs with a corresponding peak in σ_1 (16, 25). In such a case, the spectral weight would be associated with a pure superfluid response, which is certainly intriguing since our LBCO sample is (as discussed above) at ~35 K following e-ph equilibration (i.e., ~2.7 T_c). It is, however, not clear how photoexcitation could lead to uniform creation of a well-defined

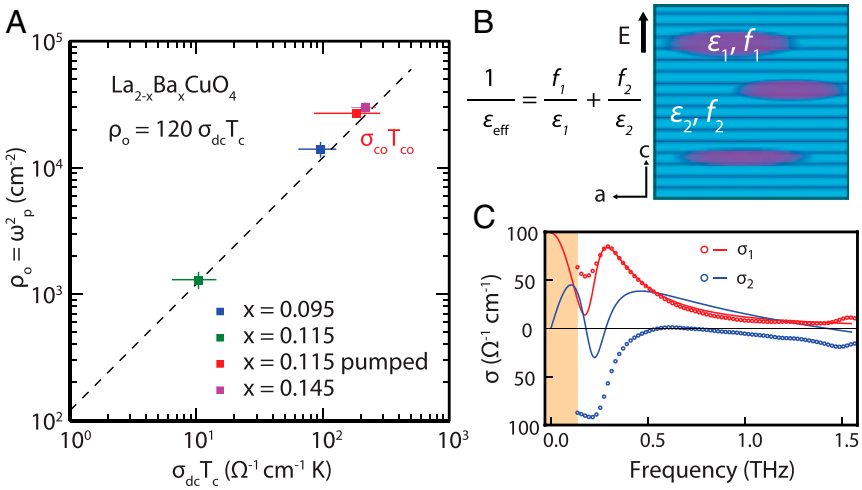

Fig. 4. (*A*) Plot of the superfluid density ρ_s versus the product of the zero-frequency conductivity (σ_{dc}) and the superconducting transition temperature T_c for several dopings of LBCO (σ_{dc} is the conductivity measured just above the superconducting transition). The values for x = 0.95 and x = 0.145 were taken from ref. 22. The dashed line is the universal scaling relation for cuprates $\rho_s = 120\sigma_{dc}T_c$ found by Homes et al. (23) (*B*) Schematic of anisotropic effective medium theory along the c axis with regions of different dielectric constants ε_1 and ε_2 and filling fractions f_1 and f_2, respectively. The superconducting volume is depicted with dark ellipses and the transformed region is in blue. (*C*) Real (red) and imaginary (blue) parts of the THz conductivity after photoexcitation with 100 μJ/cm^2 at 7 K. Experimental data are plotted with dots and the effective medium model with solid lines.

microscopic bilayer structure, although spectroscopic aspects of this are present in the non–charge-ordered LBCO (x = 0.095) (13). However, for x = 0.115, charge-order collapse plays a dominant role as described above. As such, we consider an alternative scenario based on photoinduced mesoscopic inhomogeneity.

The simplest effective medium theory for an anisotropic layered crystal (appropriate to c-axis cuprates) is schematically depicted in Fig. 4*B* where regions are transformed into a metastable state (blue) while others remain untransformed (dark ellipses). The domain boundaries of the 2 different phases are along the a-b plane giving rise to regions with differing c-axis coupling strengths. The dark horizontal stripes represent the insulating barriers between CuO_2 planes which give rise to the Josephson effect along the c axis. The effective dielectric response ε_{eff} is given as $1/\varepsilon_{eff} = f_1/\varepsilon_1 + f_2/\varepsilon_2$ where f_1 and f_2 are the volume fractions corresponding to regions with complex dielectric function ε_1 and ε_2, respectively (26). Taking f_1 as the superconducting volume fraction (having the 7 K equilibrium response), and f_2 as a Drude response (with a finite scattering rate of 0.36 THz) yields the fit to the experimental data shown in Fig. 4*C*. For additional details regarding the model and fit we refer the reader to *SI Appendix*, section S4. Notably, the peak in σ_1 corresponding to a photoinduced transverse mode is accurately reproduced with this model taking $f_1 = 0.02 \pm 0.01$ and $f_2 = 0.98 \pm 0.01$. While the general features of σ_2 are reproduced by the effective medium model, an exact fit was not possible. We note that errors in extracting σ_2 from experiment are generally more difficult in comparison to σ_1 as this depends sensitively on changes in phase of the terahertz pulse.

Taking the fits as representative of the photoinduced state leads to some interesting conclusions. First, the preponderant component consisting of a Drude response is consistent with the picture presented above that the pump destroys the charge/spin order. Second, a small but nonnegligible superconducting volume fraction (~2%) is required to obtain the spectral response in Fig. 4*C*. This indicates that even though the temperature is more than 2 times greater than the equilibrium T_c, regions of superconductivity persist. Furthermore, the Drude response (associated with f_2) is anomalous as it exhibits a small scattering rate of 0.36 THz. This is surprising for a nonsuperconducting c-axis response and has not been observed in the equilibrium c-axis response for any cuprate material. We suggest that the origin of this enhanced response arises from incipient superconducting correlations that enhance the c-axis conductivity as has been theoretically discussed (27, 28). This is consistent with the experimental observation that the observed metastability requires starting from an initial superconducting state and that a nonzero superconducting volume fraction persists after photoexcitation. Previous pump–probe studies on the cuprates have also observed long-lived dynamics after photoexcitation of the superconducting state, although the fluence dependence differs from what we have observed (29–31). In these studies the slow relaxation rate of the quasiparticles is described by a persistent phase separation along the CuO planes which may be a general feature in the cuprates and responsible for the long-lived state we observe. It will be important to pursue comparative experimental studies as a function of doping and excitation fluence and to gain additional insight into the nature of the metastability we have observed in LBCO. Such studies will also benefit from theoretical investigations of the origin of metastability in materials with competing order (32).

In summary, low-fluence photoexcitation favors the establishment of a long-lived state with superconductivity playing an important role. Additional experiments are required to fully characterize the observed metastable response and the effective medium description of mesoscale inhomogeneity that includes a superfluid response. Our results raise crucial theoretical questions including the origin of the superconductivity and the physics and surprisingly long lifetime of the metallic state. The observed long lifetime bodes well for performing additional experiments, including time-resolved nanoscopy to spatially resolve the photoinduced state.

ACKNOWLEDGMENTS. Funding from Department of Energy Basic Energy Sciences DE-SC0018218 is acknowledged. Work at Brookhaven National Laboratory was supported by the Office of Science, U.S. Department of Energy under Contract DE-SC0012704. We thank Danielle Nicoletti and Andrea Cavalleri as well as Ryo Shimano and Rysuke Matsunaga for fruitful discussions.

1. J. M. Tranquada, B. J. Sternlieb, J. D. Axe, Y. Nakamura, S. Uchida, Evidence for stripe correlations of spins and holes in copper oxide superconductors. *Nature* **375**, 561–563 (1995).
2. Q. Li, M. Hücker, G. D. Gu, A. M. Tsvelik, J. M. Tranquada, Two-dimensional superconducting fluctuations in stripe-ordered $La_{1.875}Ba_{0.125}CuO_4$. *Phys. Rev. Lett.* **99**, 067001 (2007).
3. J. Chang *et al.*, Direct observation of competition between superconductivity and charge density wave order in $YBa_2Cu_3O_{6.67}$. *Nat. Phys.* **8**, 871–876 (2012).
4. T. P. Croft, C. Lester, M. S. Senn, A. Bombardi, S. M. Hayden, Charge density wave fluctuations in $La_{2-x}Sr_xCuO_4$ and their competition with superconductivity. *Phys. Rev. B* **89**, 224513 (2014).
5. D. Basov, T. Timusk, Electrodynamics of high-Tc superconductors. *Rev. Mod. Phys.* **77**, 721–779 (2005).
6. C. Giannetti *et al.*, Ultrafast optical spectroscopy of strongly correlated materials and high-temperature superconductors: A non-equilibrium approach. *Adv. Phys.* **65**, 58–238 (2016).
7. R. Matsunaga *et al.*, Light-induced collective pseudospin precession resonating with Higgs mode in a superconductor. *Science* **345**, 1145–1149 (2014).
8. D. Fausti *et al.*, Light-induced superconductivity in a stripe-ordered cuprate. *Science* **331**, 189–191 (2011).
9. W. Hu *et al.*, Optically enhanced coherent transport in $YBa_2Cu_3O_{6.5}$ by ultrafast redistribution of interlayer coupling. *Nat. Mater.* **13**, 705–711 (2014).
10. J. I. Okamoto, W. Hu, A. Cavalleri, L. Mathey, Transiently enhanced interlayer tunneling in optically driven high- T_c superconductors. *Phys. Rev. B* **96**, 144505 (2017).
11. D. Nicoletti *et al.*, Optically induced superconductivity in striped $La_{2-x}Ba_xCuO_4$ by polarization-selective excitation in the near infrared. *Phys. Rev. B* **90**, 100503 (2014).
12. K. Tamasaku, Y. Nakamura, S. Uchida, Charge dynamics across the CuO_2 planes in $La_{2-x}Sr_xCuO_4$. *Phys. Rev. Lett.* **69**, 1455–1458 (1992).
13. S. J. Zhang *et al.*, Light-induced new collective modes in the superconductor $La_{1.905}Ba_{0.095}CuO_4$. *Phys. Rev. B* **98**, 020506 (2018).
14. D. van der Marel, A. Tsvetkov, Transverse optical plasmons in layered superconductors. *Czech. J. Phys.* **46**, 3165–3168 (1996).
15. H. Shibata, T. Yamada, Double Josephson plasma resonance in T* phase $SmLa_{1-x}Sr_xCuO_{4-d}$. *Phys. Rev. Lett.* **81**, 3519–3522 (1998).
16. T. Kakeshita *et al.*, Transverse Josephson plasma mode in T* cuprate superconductors. *Phys. Rev. Lett.* **86**, 4140–4143 (2001).
17. M. Hücker *et al.*, Stripe order in superconducting $La_{2-x}Ba_xCuO_4$ 0.095<x<0.155. *Phys. Rev. B* **83**, 104506 (2011).
18. K. Kumagai, H. Matoba, N. Wada, M. Okaji, K. Nara, Some anomalies due to the low-temperature structural transition around x=0.12 in $La_{2-x}Ba_xCuO_4$. *J. Phys. Soc. Jpn.* **60**, 1448–1451 (1991).
19. M. Fujita, H. Goka, K. Yamada, M. Matsuda, Competition between charge- and spin-density-wave order and superconductivity in $La_{1.875}Ba_{0.125-x}Sr_xCuO_4$. *Phys. Rev. Lett.* **88**, 167008 (2002).
20. J. M. Tranquada *et al.*, Evidence for unusual superconducting correlations coexisting with stripe order in $La_{1.875}Ba_{0.125}CuO_4$. *Phys. Rev. B.* **78**, 1–13 (2008).
21. S. Tajima, T. Noda, H. Eisaki, S. Uchida, C-axis optical response in the static stripe ordered phase of the cuprates. *Phys. Rev. Lett.* **86**, 500–503 (2001).
22. C. C. Homes *et al.*, Determination of the optical properties of $La_{2-x}Ba_xCuO_4$ for several dopings, including the anomalous x=1/8 phase. *Phys. Rev. B* **85**, 134510 (2012).
23. C. C. Homes *et al.*, A universal scaling relation in high-temperature superconductors. *Nature* **430**, 539–541 (2004).
24. Q. Jie, S. J. Han, I. Dimitrov, J. M. Tranquada, Q. Li, Transport properties of stripe-ordered high Tc cuprates. *Phys. C Supercond.* **481**, 46–54 (2012).
25. D. van der Marel, A. A. Tsvetkov, Transverse-optical Josephson plasmons: Equations of motion. *Phys. Rev. B* **64**, 024530 (2001).
26. G. W. Milton, *The Theory of Composites* (Cambridge University Press, 2002), p. 195.
27. L. G. Aslamazov, A. I. Larkin, The influence of fluctuation pairing of electrons on the conductivity of normal metal. *Phys. Lett.* **26**, 238–239 (1968).
28. M. H. Redi, Two-dimensional fluctuation-induced conductivity above the critical temperature. *Phys. Rev. B* **16**, 2027–2031 (1977).
29. G. Yu, C. H. Lee, A. J. Heeger, S.-W. Cheong, Z. Fisk, Photo-excitation of single crystals of $La_2CuO_{4+\delta}$ near the metal-insulator transition. *Phys. C Supercond.* **190**, 563–568 (1992).
30. P. Kusar *et al.*, Controlled vaporization of the superconducting condensate in cuprate superconductors by femtosecond photoexcitation. *Phys. Rev. Lett.* **101**, 227001 (2008).
31. P. Kusar *et al.*, Dynamical structural instabilities in $La_{1.9}Sr_{0.1}CuO_4$ under intense laser photoexcitation. *J. Supercond. Nov. Magn.* **24**, 421–425 (2010).
32. Z. Sun, A. J. Millis, Transient trapping into metastable states in the systems with competing orders. arXiv:1905.05341v1 [cond-mat.str-el] (14 May 2019).

PNAS
www.pnas.org

Supplementary Information for

Photo-enhanced metastable c-axis electrodynamics in striped ordered cuprate $La_{1.885}Ba_{0.115}CuO_4$

K. A. Cremin[1], J. Zhang[1,2], C. C. Homes[3], G. D. Gu[3], Z. Sun[1,4], M. M. Fogler[1], A. J. Millis[4,5], D. N. Basov[4], R.D. Averitt[1]

[1]*Department of Physics, University of California San Diego, La Jolla, CA 92093*

[2]*Department of Physics, Hong Kong University of Science and Technology, Clear Water Bay, Kowloon, Hong Kong, China*

[3]*Condensed Matter Physics and Materials Science Department, Brookhaven National Laboratory, Upton, New York 11973*

[4]*Department of Physics, Columbia University, New York, New York 10027*

[5]Center for Computational Quantum Physics, Flatiron Institute, New York, NY 10010

Richard Averitt

Email: raveritt@ucsd.edu

This PDF file includes:

Supplementary text

Figs. S1 to S5

References for SI reference citations

www.pnas.org/cgi/doi/10.1073/pnas.1908368116

Supplementary Information Text

S1: Methods

The $La_{1.885}Ba_{0.115}CuO_4$ (LBCO) crystal studied was cut and polished to expose the *ac* surface with a large area of 5 mm x 5 mm. The c-axis properties were probed with broadband THz pulses generated from a commercial GaAs based photo-conductive antenna using incident light from a 1 kHz Ti:Sapphire regenerative amplifier. The THz pulses produced have a usable bandwidth from 0.15-2 THz which allowed a measurement of the equilibrium Josephson plasma resonance (JPR) near 0.2 THz for x = 0.115 doping. Figure S1 shows a schematic of the optical pump-THz probe measurement in reflection.

The probe pulses were focused onto the sample at an incident angle of 30 degrees with the electric field polarized along the c-axis. The THz pulses were collected after the sample and measured via electro-optic sampling with an 800 nm gate pulse in a 2mm thick ZnTe crystal. The LBCO crystal was photoexcited with 100 fs, 800 nm wavelength pulses, polarized along the c-axis with a beam diameter of 6 mm FWHM to ensure a uniform excitation across the sampled region.

The equilibrium c-axis reflectivity above T_c was characterized with broadband FTIR measurements at 30 K which is displayed in Fig. S2. The equilibrium complex index of refraction $n(\omega)$ was determined by fitting the reflectivity curve with Drude-Lorentz oscillators placed at known IR phonon frequencies[1]. The fit was accomplished using the software package RefFIt^{TM} and is shown in Fig. S2. A small Drude component was added

to give a dc conductivity $\sigma_1(\omega=0) \sim 3\ \Omega^{-1}cm^{-1}$ at 30 K to match previous transport measurements[1,2].

The reflection coefficient of a material is given by $r(\omega) = E_s(\omega)/E_i(\omega)$ where $E_s(\omega)$ is the electric field reflected off the sample and $E_i(\omega)$ is the incident field. By measuring the THz waveform $E_s(t)$ via electro-optic sampling, we take the Fourier transform to obtain $E_s(\omega)$. The reflection coefficient was then determined at 7 K by measuring $E_{s,7K}(\omega)$ and using the relation

$$r_{7\mathrm{K}} = \frac{E_{s,7\mathrm{K}}(\omega)}{E_{s,30\mathrm{K}}(\omega)} r_{30\mathrm{K}} \quad (1)$$

where r_{30K} is the reflection coefficient obtained from the Drude-Lorentz fitting. Figure S2(b)(c) displays a measurement of the single cycle THz pulses reflected from the sample at 30 K and 7 K in the time domain and frequency domain respectively.

S2: Layer Model and parameter extraction

The photo-induced change $\Delta E_s(t,\tau)$ in the reflected electric field was measured at various pump probe time delays τ, over the temporal window t of the THz pulse. The quantity $\Delta E_s(t,\tau) = E_{s,pumped}(t,\tau) - E_{s,unpumed}(t,\tau)$ was acquired at each delay time τ by using a lock-in triggered by the modulation of the pump pulse with a mechanical chopper. The unpumped electric field was measured 40 ps before the arrival of the pump pulse.

The raw photo-induced changes ΔE measured in the reflected field require further processing to extract the complex optical properties of the excited region. The penetration depth mismatch between 800 nm pump (~400 nm) and THz probe (~100-300 μm) results

in a relatively small change in ΔE (~1-3 %) after photo-excitation and is considered when modeling the THz response. We model the photo-excited region as a thin layer with a thickness of d = 400 nm on top of an unperturbed bulk containing the material properties of the sample in equilibrium before the arrival of the pump pulse. The total complex reflection coefficient $r'(\omega)$ from the layered system is the summation of all internal reflections displayed in Fig. S3 and can be expressed in closed form as:[3]

$$r'(\omega) = \frac{r_{01}+r_{12}e^{i2\delta}}{1+r_{01}r_{12}e^{i2\delta}}, \quad (2)$$

$$\delta = \frac{2\pi d}{\lambda}\sqrt{n_1^2 - \sin^2\theta_1} \quad (3)$$

where r_{01} and r_{12} are the reflection coefficients from the front and backside of the excited layer, respectively, and λ is the THz wavelength. The phase accumulation as the THz pulse travels through the excited layer is given by δ. The complex reflection coefficient $r'(\omega,\tau)$ was determined from the experimentally measured quantities $\Delta E_s(\omega,\tau)$ and $E_s(\omega)$ using the relation $r'(\omega,\tau) = r(\omega)[\Delta E_s/E_s + 1]$ where $r(\omega)$ is the equilibrium reflection coefficient. A numerical solution to the above Fresnel equation was found, returning a value for the complex index of refraction $n_1(\omega,\tau)$ of the excited layer. We calculate the complex conductivity of the photo-excited layer

$$\sigma(\omega,\tau) = \frac{\omega}{4\pi i}[n_1(\omega,\tau)^2 - \varepsilon_\infty], \quad (4)$$

using ε_∞ = 4.5 as a standard value for the cuprates[4]. The photo-excited reflectivity plotted in Fig. (2) and (3) in the main text were recalculated using the complex index of refraction $n_1(\omega,\tau)$.

S3: Pump induced heating

Heating effects are present in all pump probe measurements and the effective lattice temperature must be considered after photo-excitation. We use a two-temperature model to estimate the final lattice temperature after electron-phonon thermalization has occurred (in ~1ps). The specific heat for $La_{2-x}Ba_xCuO_4$ is described by the relation

$$C_s = \gamma T + \beta T^3 \quad (5)$$

over a wide temperature range[5], where γ and β are the electronic and lattice coefficients to the specific heat, respectively. Specific heat coefficients were taken as γ ~ 2.5 mJ mol^{-1} K^{-2} and β ~ 0.25 mJ mol^{-1} K^{-4} estimated from literature values of nearby dopings[5]. For a given pump fluence we estimate the absorbed energy over the photo-excited region and calculate the effective temperature after electron phonon-thermalization by integrating

$$Q_{\text{pump}} = \int_{T_i}^{T_f} N C_s(T) dT \ , \quad (6)$$

where Q_{pump} is the total energy absorbed from the pump pulse, N is the number of moles in the excited volume, T_i is the initial temperature and T_f is the final temperature after electron-phonon thermalization. The absorbed energy Q_{pump} is estimated by $Q_{\text{pump}} = F^*A(1-R)$ where F is the pump fluence, A is the area of the pump beam on the sample using the FWHM (~6 mm) as the diameter, and R is the reflectivity at 1.55 eV which is ~ 0.15[1]. The excited volume is estimated as a cylindrical disk with a diameter of 6 mm and height equal to the penetration depth.

The final temperature T_f is calculated numerically and plotted versus pump fluence in Fig. S4 for an initial temperature T_i = 7 K. The colored points correspond to the various fluences used in the experiment and the $\Delta E/E$ pump probe traces displayed in the inset.

S4: Effective medium model

We model the photo-excited layer in LBCO as inhomogeneous where regions are transformed into a metastable state while the remaining stays untransformed. The most simplified model is depicted in figure 4(b) of the main text where domain boundaries of the two phases are along the a-b plane. If the typical length scale of the inhomogeneity is much smaller than the thickness *d* of the photo-excited layer, one could treat the latter as a 3D uniform medium whose dielectric function along the c-axis is described by the effective medium formula[6]

$$\frac{1}{\varepsilon_{\text{eff}}} = \frac{f_1}{\varepsilon_1} + \frac{f_2}{\varepsilon_2}\,, \tag{6}$$

where ε_{eff} is the effective dielectric function,

$$\varepsilon_1 = \varepsilon_\infty \left(1 - \frac{\omega_{j1}^2}{\omega^2}\right) + \frac{4\pi i}{\omega}\sigma_t\,, \tag{7}$$

$$\varepsilon_2 = \varepsilon_\infty \left(1 - \frac{\omega_{j2}^2}{\omega(\omega + i\gamma_2)}\right) \tag{8}$$

are the dielectric functions of the original and transformed regions with corresponding volume fractions $f_1$and $f_2$respectively. Eq. (7) describes the optical conductivity of a Josephson array imbedded in a dielectric environment $\varepsilon_\infty$with ω_{j1}being the strength of the equilibrium JPR and $\sigma_t$the dissipative interlayer tunneling conductivity. The

transformed region is described by a Drude type response in Eq. (8) with plasma strength ω_{j2} and scattering rate γ_2.

The experimental data (red and blue dots) and effective medium model (solid curves) are plotted in Fig. S5 in terms of the optical conductivity. The values of the parameters used in the model are: ω_{j1}= 1.8 THz, σ_t= 0.38 Ω^{-1}cm^{-1}, f_1= 0.22, ω_{j2} = 1.45 THz, γ_2= 0.26 THz, f_2= 0.978 and ε_∞= 30. The difference in filling fractions suggests that most of the excited layer is transformed but a small remaining superconducting fraction is necessary to match the experimental results. The dashed lines in Fig. S5 are the model plotted with a ±1% difference in filling fractions which is taken to be the error on $f_1$and f_2.

Figures

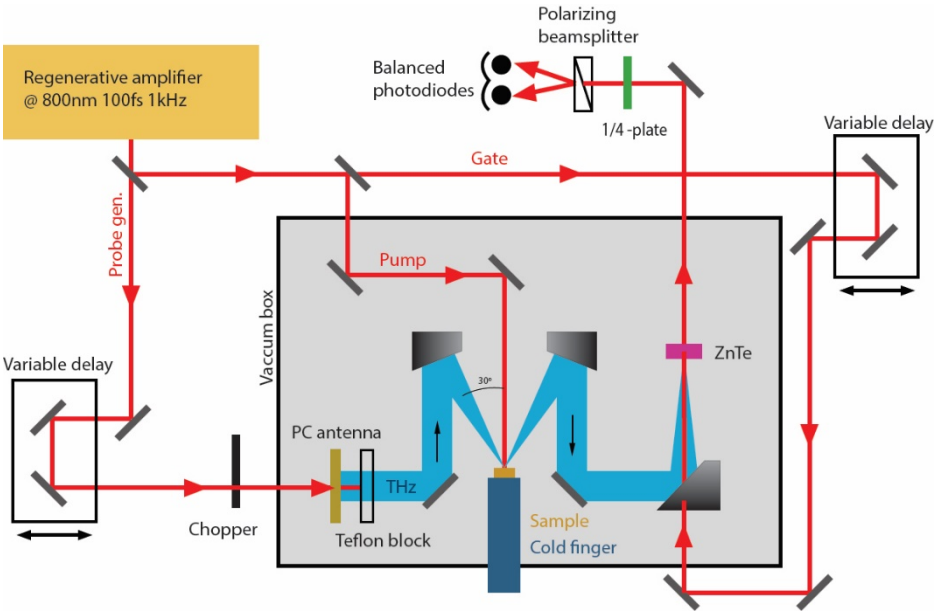

Fig. S1. Schematic of experimental setup for near-IR pump THz probe.

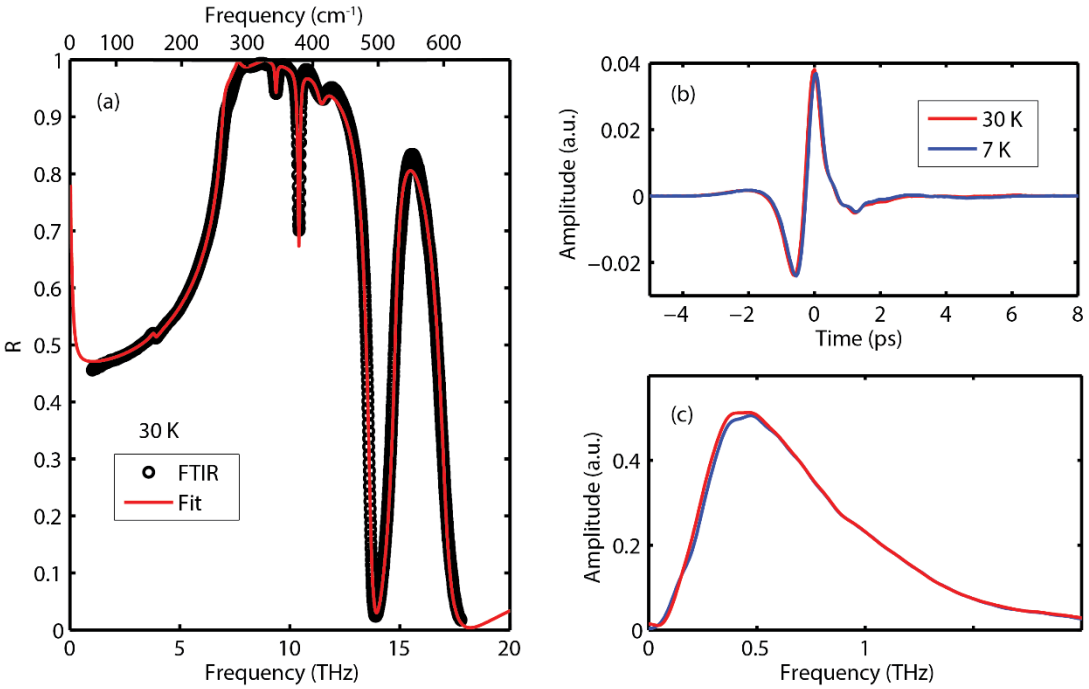

Fig. S2. (a) c-axis reflectivity FTIR data taken at 30K with fit. (b) Time domain profile of THz pulse reflected from the sample at 30 K and 7 K. (c) Fourier transform of the time domain pulses in panel (b).

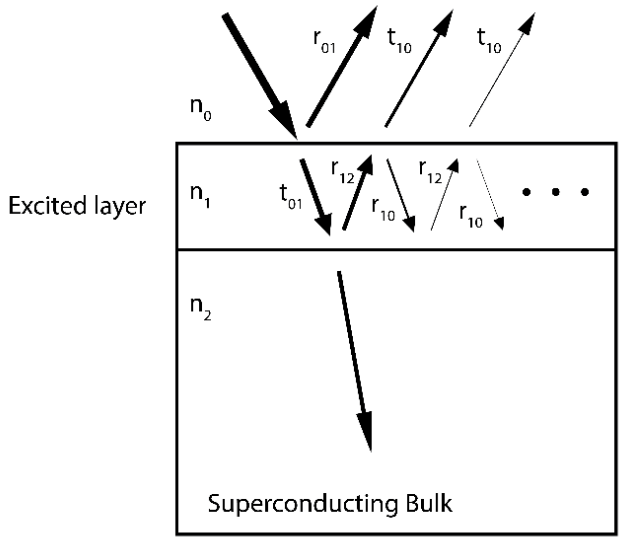

Fig. S3. Schematic drawing of thin layer model. In this model the thin excited layer sits on top of the bulk crystal containing the equilibrium optical properties.

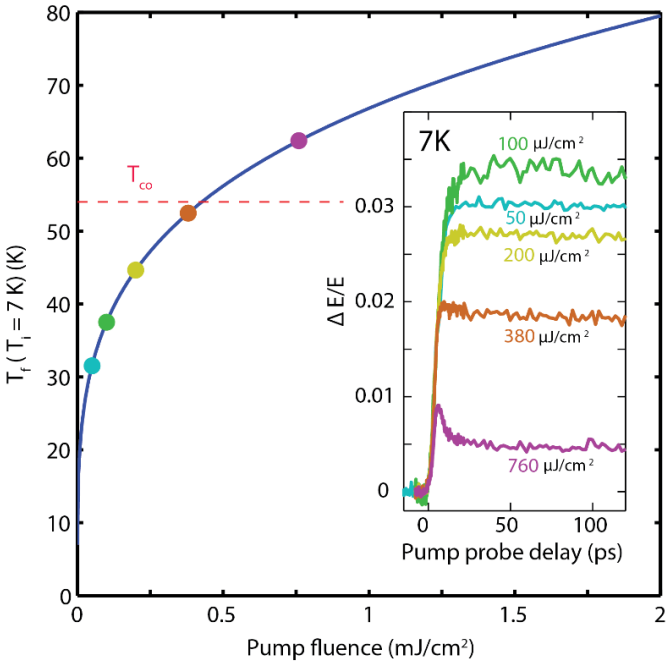

Fig. S4. Calculated final lattice temperature after electron-phonon thermalization. The colored dots represent T_f for a given fluence which are color coordinated with the inset figure. The inset is the time dependent relative change in the THz electric field amplitude after excitation at various pump fluences (at 7 K). The red dashed line is the charge order transition temperature T_{co}.

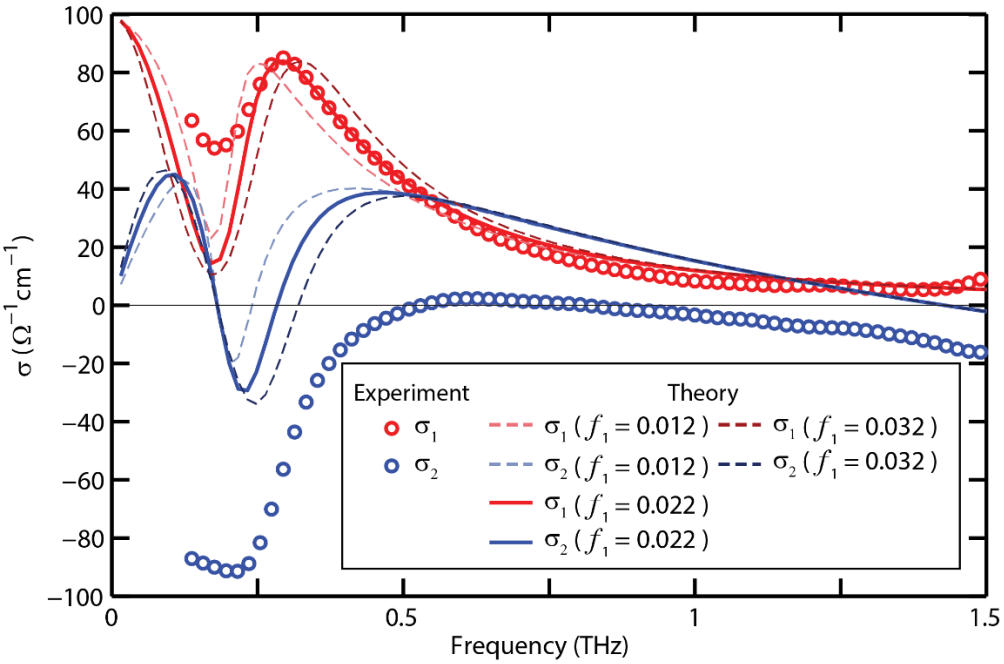

Fig. S5. Optical conductivity of the photo-excited meta-stable phase in LBCO at 7K. The red and blue dots are experimental data and the solid and dashed lines are the optical conductivity calculated from the effective medium model with varying values of the filling fractions. The model shown in Fig. 4(c) of the main text is the same as the solid curve plotted here.

References:

1. C. C. Homes, *et al.*, Determination of the optical properties of $La_{2-x}BaxCuO_4$ for several dopings, including the anomalous x=1/8 phase. *Phys. Rev. B* **85**, 134510 (2012).
2. Q. Jie, S. J. Han, I. Dimitrov, J. M. Tranquada, Q. Li, Transport properties of stripe-ordered high T_c cuprates. *Phys. C* **481**, 46–54 (2012).
3. M. Dressel, G. Gruner, *Electrodynamics of Solids*. (Cambridge University Press, 2002).
4. T. C. Choy. *Effective medium theory: principles and applications*. (Oxford University Press, 1999).
5. Y. Okajima, K. Yamaya, N. Yamada, M. Oda, M. Ido, Reduction of the electronic coefficient of the specific heat around x=0.065 in $(La_{1-x}Ba_x)_2CuO_4$. *Solid State Commun.* **74**, 767–771 (1990).
6. G. W. Milton, *The Theory of Composites* (Cambridge University of Press, Cambridge, England, 2002).